

Two-Dimensional Electronic-Vibrational Sum Frequency Spectroscopy for Interactions of Electronic and Nuclear Motions at Interfaces

Gang-hua Deng¹, Yuqin Qian¹, Tong Zhang¹, Jian Han¹, Hanning Chen², and Yi Rao^{1*}

¹Department of Chemistry and Biochemistry, Utah State University, Logan, UT 84341, USA

²Department of Chemistry, American University, Washington, DC 20016, USA

*Corresponding author: Yi Rao

Email: yi.rao@usu.edu

Author Contributions: Y.R. designed research; G.H.D. and Y.Q.Q performed research; Y.R., Y.Q.Q, T.Z, and G.H.D. analyzed data, J.H. synthesized samples; H.N.C. contributed to theoretical calculations; Y.R., Y.Q.Q, and H.N.C. wrote the paper.

Competing Interest Statement: The authors declare no competing interest.

Classification: Physical Sciences (Chemistry)

Keywords: Electronic-vibrational couplings; sum frequency generation; two-dimensional spectroscopy; excited sates at interfaces; interfacial chemistry

Abstract

Interactions of electronic and vibrational degrees of freedom are essential for understanding excited states relaxation pathways of molecular systems at interfaces and surfaces. Here we present the development of interface-specific two-dimensional electronic-vibrational sum frequency spectroscopy (2D-EVSFG) for electronic-vibrational couplings for excited states at interfaces and surfaces. We demonstrate this 2D-EVSFG technique by investigating photoexcited interface-active AP3 molecules at the air/water interface as an example. Our 2D-EVSFG experiments show strong vibronic couplings of interfacial AP3 molecules upon photoexcitation and subsequent relaxation of a locally excited (LE) state. Time-dependent 2D-EVSFG experiments indicate that the relaxation of the LE state, S_2 , is strongly coupled with two high-frequency modes of 1529.1 cm⁻¹ and 1568.1 cm⁻¹. Quantum chemistry calculations further verify that the strong vibronic couplings of the two vibrations promote the transition from the S_2 state to the lower excited state S_1 . We believe that this development of 2D-EVSFG opens up a new avenue of understanding excited state dynamics related to interfaces and surfaces.

Significance Statement

Electronic-vibrational couplings are pivotal in many photo-induced processes at interfaces and surfaces. Two-dimensional electronic-vibrational sum frequency spectroscopy (2D-EVSFG) is a unique tool to decipher electronic-vibrational couplings for excited states of molecules at interfaces and surfaces, enabling the correlation of photo-induced electronic-vibrational manifolds with their subsequent time evolution of high-frequency vibrational modes. This technique is especially powerful to monitor ultrafast processes such as charge transfer, energy transfer, proton transfer, and proton-coupled charge transfer at interfaces and surfaces on a real-time basis.

Introduction

Electronic and vibrational degrees of freedom are the most important physical quantities in molecular systems at interfaces and surfaces. Knowledge of interactions between electronic and vibrational motions, namely electronic-vibrational couplings, is essential to understanding excited states relaxation pathways of molecular systems at interfaces and surfaces. Many excited states relaxation processes occur at interfaces and surfaces, including charge transfer, energy transfer, proton transfer, proton-coupled electron transfer, and configurational dynamics as so on.(1-11) These relaxation processes are intimately related to the electronic-vibrational couplings at interfaces and surfaces. Strong electronic-vibrational couplings could promote nonadiabatic evolution of excited potential energy, and thus facilitate chemical reactions or intramolecular

structural changes of interfacial molecules.(10, 12, 13) Furthermore, these interactions of electronic and vibrational degrees of freedom are subject to solvent environments, e.g., interfaces/surfaces with restricted environment of unique physical and chemical properties.(9, 14, 15) Despite the importance of interactions of electronic and vibrational motions, little is known about excited-state electronic-vibrational couplings at interfaces and surfaces.

Interface-specific electronic and vibrational spectroscopies enable us to charaterize the electronic and vibrational structures, separately. As interface-specific tools, second-order electronic sum frequency generation (ESFG) and vibrational sum frequency generation (VSFG) spectroscopies have been utilized for investigating molecular structure, orientational configurations, chemical reactions, chirality, static potential, environmental issues, and biological systems at interfaces and surfaces. (16-52) Recently, structural dynamics at interfaces and surfaces have been explored using time-resolved ESFG (TR-ESFG) and time-resolved VSFG (TR-VSFG) with a visible pump or an IR pump thanks to the development of ultrafast lasers. (6-9, 13-15, 49, 53-61) Doubly resonant SFG has been demonstrated to probe both electronic and vibration transitions of interfacial molecular monolayer. (15, 62-71) This frequency-domain two-dimensional interface/surface spectroscopy could provide information regarding electronic-vibrational coupling of interfacial molecules. However, contributions from excited states are too weak to be probed due to large damping rates of vibrational states in excited states. (62, 63) As such, the frequency-domain doubly resonant SFG is used only for electronic-vibrational coupling of electronic ground states. Ultrafast interface-specific electronic-vibrational spectroscopy could allow us to gain insights into how specific nuclear motions drive the relaxation of electronic excited states. Therefore, development of interface-specific electronic-vibrational spectroscopy for excited states is needed.

In this work, we integrate the specificity of interfaces and surfaces into the capabilities of ultrafast two-dimensional spectroscopy for dynamical electronic-vibrational couplings in excited states of molecules. Two-dimensional interface-specific spectroscopies are analogous to those 2D spectra in bulk that spread the information contained in a pump-probe spectrum over two frequency axes. Thus, one can better interpret congested one-dimensional signals. 2D vibrational SFG (2D-VSFG) spectroscopy was demonstrated a few year ago.(72-74) Furthermore, heterodyne 2D-VSFG spectroscopy using mid-IR pulse shaping and noncollinear geometry 2D-VSFG experiments have been also developed to study vibrational structures and dynamics at interfaces.(31, 75-78) Recently, two-dimensional electronic sum frequency generation spectroscopy (2D-ESFG) has been also demonstrated for surfaces and interfaces.(79) On the other hand, bulk two-dimensional electronic-vibrational spectroscopy (2D-EV) has been extensively used to investigate the electronic relaxation and energy transfer dynamics of molecules, biological systems, and nanomaterials.(80-90) The 2D-EV technique not only provides electronic and vibrational interactions between excitons

or different excited electronic states of systems, but also identifies fast nonradiative transitions through nuclear motions in molecules, aggregations, and nanomaterials. However, an interface-specific technique for 2D electronic-vibrational sum frequency generation (2D-EVSFG) spectroscopy has yet to be developed.

Here we present the development of 2D-EVSFG spectroscopy for the couplings of electronic and nucleic motions at interfaces and surfaces. The purpose of developing 2D-EVSFG spectroscopy is to bridge the gap between the visible and IR regions to reveal how structural dynamics for photoexcited electronic states are coupled with vibrations at interfaces and surfaces. As an example, we applied this new 2D-EVSFG experimental method into time evolution of electronic-vibrational couplings at excited states of interface-active molecules at the air/water interface.

Theoretical Considerations. A reflection-geometry configuration for 2D-EVSFG, analogous to that for 2D-ESFG, (79, 91) is considered for studies of interfaces and surfaces, as schematically shown in Figure 1(A). There are four beams in the 2D-EVSFG experiment, and they are two femtosecond visible pump beams (E_{P1} and E_{P2}), a femtosecond middle infrared (mid-IR) beam (E_{IR}), and a picosecond 800 nm beam (E_{ps}). Both the energy and momentum of the radiated 2D-EVSFG are conserved to afford $(\mp k_{p1} \pm k_{p2} + k_{IR} + k_{ps})$ in a directional manner. The time delays of our four laser pulses are measured as the temporal gap between the maxima of the pulse envelopes, which are denoted as τ_1 , T_w , and τ_3 , respectively. Here we retain T_w instead of τ_2 for the customary reason. Moreover, the corresponding time delays between the four light-matter coupling are designated as t_1' , t_2' , t_3' , and t_4' , respectively (Figure 1(B)). Specifically, the first electric field, $E_{\rm P1}$, initiates a coherent superposition of the ground and excited electronic states. Then, the already perturbed system is populated by a second pulse into either the ground or excited state after a coherent time, τ_1 (Figure 1(C)). Subsequently, the vibrational response of the selected state is generated by the mid-IR beam with a waiting time, T_w . Finally, the non-resonant picosecond beam upconverts the vibrational polarization of the system, thus giving rise to a 2D-EVSFG signal at time t. The 2D-EVSFG electric field is written as follows, (76, 79, 91, 92)

$$E^{(4)}(t) \propto <\alpha \mu_{V3} \mu_{E1} \mu_{E2} > \int_0^\infty dt_4' \int_0^\infty dt_3' \int_0^\infty dt_2' \int_0^\infty dt_1' E_{ps}(t - t_4') E_{IR}(t + \tau_3 - t_4' - t_3') E_{p2}(t + \tau_3 + t_4' - t_3' - t_2') E_{p1}(t + \tau_3 + t_4' - t_3' - t_2' - t_1') R^{(4)}(t_4', t_3', t_2', t_1')$$

(1)

where $R^{(4)}(t_4', t_3', t_2', t_1')$ is a fourth-order response function. where μ_{E1} and μ_{E2} are the electronic dipole moment operators for the visibly resonant beams (1 & 2), μ_{V3} is the vibrational dipole moment operator, α is the transition polarizability, and the trace <...> denotes the statistically orientational

average over both the electronic and vibrational manifolds. The electronic responses of molecules interacting with a non-resonant visible light is instantaneous, it enables us to make an approximation that a Dirac delta function is applied.(76, 93) The fourth-order response function is further expressed as, (76)

$$R^{(4)}(t_4', t_3', t_2', t_1') = R^{(3)}(t_3', t_2', t_1') \cdot \delta(t_4')$$
(2)

Substitution of Eqn. 2 into Eqn.1 yields the form

$$E^{(4)}(t) \propto <\alpha \mu_{V3} \mu_{E1} \mu_{E2} > E_{ps}(t) \int_0^\infty dt_3' \int_0^\infty dt_2' \int_0^\infty dt_1' E_{IR}(t + \tau_3 - t_3') E_{p2}(t + \tau_3 + T_w - t_3' - t_2') E_{p1}(t + \tau_3 + T_w + \tau_1 - t_3' - t_2' - t_1') R^{(3)}(t_3', t_2', t_1')$$
(3)

The semi-impulsive approximation applies if an E(t) is short, namely, $\delta(t)$, when compared with the time delays between the laser pulses. As a result, we could greatly simplify Eqn.1 by eliminating the integrals of E_{p1} , E_{p2} , and E_{IR} , which is further simplified as, (76, 92)

$$E^{(4)}(t, T_w, \tau_1; \tau_3) \propto <\alpha \mu_{V3} \mu_{E1} \mu_{E2} > E_{nS}(t - \tau_3) E_{IR} E_{n2} E_{n1} R^{(3)}(t, T_w, \tau_1)$$
(4)

A spectrometer implements direct Fourier transformation from t to the detection frequency, ω_t . The 2D-EVSFG electric field takes the form,

$$E^{(4)}(\omega_t, T_w, \tau_1; \tau_3) \propto <\alpha \mu_{V3} \mu_{E1} \mu_{E2} > E_{IR} E_{v2} E_{v1} E_{vs}(\omega_{vis}; \tau_3) \otimes R^{(3)}(\omega_{IR}, T_w, \tau_1)$$
(5)

where ω_t is the energy of sum frequency, $\omega_{SFG} = \omega_{vis} + \omega_{IR}$. Thus, this renders the convolution of the narrow band E_{ps} with the response function.(93) As a matter of fact, the temporally wide picosecond pulse E_{ps} serves as a window function in this case.(76, 93) Eventually, a frequency domain 2D-EVSFG spectrum $E^{(4)}(\omega_{SFG}, T_w, \omega_\tau; \tau_3)$ is the Fourier transformation to excitation frequency, ω_τ , from the experimentally measured 2D spectra, $E^{(4)}(\omega_{SFG}, T_w, \tau_1; \tau_3)$ for a given waiting time, T_w . We will neglect the time delay between the IR and the picosecond pulse, τ_3 , thereafter since it is here fixed.

To elucidate how electronic and vibrational transitions of molecules at interfaces and surfaces take place in the 2D-EVSFG, we shall examine two vibronic states with different curvatures and equilibrium position displacements, d, relative to the ground state as our model system. Figure 1(C) schematically projects a three-dimensional excited state potential, S_1 , into possible vibronic transitions ($gv \rightarrow eu'$ and $gv \rightarrow e'u''$), leading to a frequency shift in vibrational modes, $\Delta_{11'} = \omega_{0'1'}$. The $R^{(4)}(t'_4, t'_3, t'_2, t'_1)$ of a molecule at interfaces and surfaces follows the Feynman pathways as shown in Figure 1(D), which present four possible rephasing pathways for the eu' vibronic state (I for GSB & II for ESA) and for the e'u'' vibronic state (I' for GSB & II' for ESA). From an

experimental perspective, the pure adsorptive 2D-EVSFG acquired in a pump-probe geometry consists of its both rephasing and non-rephasing pathways.(94)

2D-EVSFG signal stems from the negative components of ground state bleaching (GSB) and the positive components of excited state absorption (ESA). As a result, the interface-specific EV polarization is composed of two parts: one from the GSB and the other from the ESA. $R^{(3)}(t, T_w, \tau_1)$ is proportional to the line shape function, $F(t, T_w, \tau_1)$, based upon the basic principle of nonlinear optical spectroscopy, (76, 79, 91, 92) Accordingly, the fourth-order GSB and ESA polarizations are written as,

$$E_{GSB}^{(4)}(t, T_w, \tau_1) \propto <\alpha_{qv',qv}\mu_{q,v,qv'}\mu_{qv,eu}\mu_{qv,eu} > F_{GSB}(t, T_w, \tau_1)$$
(6)

and

$$E_{ESA}^{(4)}(t, T_w, \tau_1) \propto <\alpha_{eu',eu}\mu_{eu,eu'}\mu_{gv,eu}\mu_{gv,eu} > F_{ESA}(t, T_w, \tau_1)$$
(7)

Figure 1(E) schematically demonstrates how 2D-EVSFG peaks are distributed over both the negative GSB and positive ESA of interfacial molecules upon photoexcitation. These peaks correspond to the two vibronic transitions for the four Feynman pathways in Figure 1(D).

Similar to the femtosecond stimulated Raman scattering,(95-98) and two-dimensional electronic-Raman spectroscopy,(99) 2D-EVSFG employs one or two acting pumps as well as two probe pulses (one picosecond pulse plus an white light or IR). Nevertheless, 2D-EVSFG distinguishes itself as a fourth-order wave-mixing process that leads to interface/surface specificity by detecting an up-conversion frequency mixing of the IR probe with the picosecond laser. By contrast, both the femtosecond stimulated Raman scattering and two-dimensional electronic-Raman spectroscopy are driven by a fifth-order nonlinear response dominantly contributed from the bulk phase.

Results

Linear and SFG spectra of AP3. We shall begin to characterize linear optical properties of AP3. The chemical structure of AP3 ((*E*)-4-((4-(dihexylamino) phenyl)diazinyl)-1-methylpyridin-1-lum) is displayed in the inset of Figure 2(A). In AP3, the donor and acceptor moieties are distributed at the amino- and pyridinium- groups, respectively. Figure 2(A) presents UV spectrum of 100 μM AP3 in water, which maximum absorption peak is located at 575 nm with an asymmetric shoulder. The IR spectrum of AP3 displays seven peaks at 1416 cm⁻¹, 1464 cm⁻¹, 1503 cm⁻¹, 1521 cm⁻¹, 1543 cm⁻¹, 1599 cm⁻¹, and 1626 cm⁻¹ in Figure 2 (B). On the other hand, the Raman spectrum of AP3 shows

that four peaks appear at 1419 cm⁻¹, 1502 cm⁻¹, 1601 cm⁻¹, and 1639 cm⁻¹ from 1350 to 1800 cm⁻¹ in Figure 2 (C).

Vibrational SFG spectra of 20 μM AP3 from the air/water interface were taken over 1350 -1800 cm⁻¹. Figure 2(D) shows two dominant peaks at 1608.9 cm⁻¹ and 1631.1 cm⁻¹. On the other hand, two weak and broad peaks occur at 1496.2 cm⁻¹ and 1551.8 cm⁻¹. A VSFG-active mode is known to be both Raman and IR active. The three VSFG-active modes of 1496.2 cm⁻¹, 1608.9 cm⁻¹ ¹, and 1631.1 cm⁻¹ are both Raman and IR active. Only one VSFG peak at 1551.8 cm⁻¹ is IR active only. To understand the nature of these four vibrational modes, quantum chemistry calculations were carried out. The calculated Raman and IR spectra are displayed in Figure S1. Compared with those modes for the IR and Raman of AP3, the four VSFG-active modes of 1496.2 cm⁻¹, 1551.8 cm⁻¹, 1608.9 cm⁻¹, and 1631.1 cm⁻¹ were assigned to the ring-breathing mode, in-plane bending mode, ring-scissoring mode predominantly on benzene, and ring-scissoring mode predominantly on pyridinium, respectively. All of the four vibrational modes are visualized in Figure S2. As shown in our simulated spectra of AP3 in Figure S1, the vibrational mode centered at ca. 1570 cm⁻¹ is both IR and Raman active, even though its relative Raman intensity is significantly weaker than its IR counterpart. Experimentally, some weak but apparently non-zero Raman signal in Figure 2 (C) was also present between 1502 cm⁻¹ and 1601 cm⁻¹, leading to SFG signals in the help of the notable IR intensity in Figure 2 (B).

2D-EVSFG spectra at initial photoexcitation. Figure 3 shows 2D-EVSFG spectra of 20 μ M AP3 molecules at the air/water interface for a waiting time T_w of 20 fs. We depicted the spectral features from two aspects as follows:

- A) Along the vibrational ω_t axis, four negative peaks appear at ω_t =1462.9 cm⁻¹, 1550.6 cm⁻¹, 1606.4 cm⁻¹, and 1630.8 cm⁻¹, which were attributed to their ground state bleaching (GSB). Only one positive peak occurs at ω_t =1403.2 cm⁻¹, which was due to the vibrational transition of 1462.9 cm⁻¹ in the excited state of AP3. The spectral red shift of vibrational transitions between the GSB and ESA, Δ_{11} , was found to be 59.3 cm⁻¹. Such a significant spectral shift indicates a larger and more diffusive curvature of potential energy in the LE state of AP3 than that in its ground state. Figure 3(B) shows vibrational spectra at 570.5 nm and 559.1 nm. The vibrational spectrum at 559.1 nm shows blue shifted at the peaks of 1403.2 cm⁻¹ and 1462.9 cm⁻¹ but red shifted at the peaks of 1550.6 cm⁻¹, 1606.4 cm⁻¹, and 1630.8 cm⁻¹, with respect to those at 570.5 nm. These results suggest that 2D-EVSFG could provide information about curvatures of potential energy for different vibronic states.
- B) Along the electronic ω_{τ} axis, both the negative GSB and positive ESA spectra constitute vibronic transitions (VT) that dominate interfacial electronic absorption of AP3. For the negative

GSB spectra, two main VT peaks occur at 570.5 nm and 559.1 nm in the vibrational modes of 1462.9 cm⁻¹, 1550.6 cm⁻¹, 1606.4 cm⁻¹, and 1630.8 cm⁻¹. The interfacial absorption peak at the lowest energy of 570.5 nm is blue shifted with respect to the visible absorption in bulk water for AP3 (Figure 2(A)). The blue shift in the interfacial spectrum could be understood by the hydrophobic nature of the air/water interface. Unlike the broad and featureless electronic spectra in bulk, the interfacial electronic spectrum of AP3 exhibits two discernible VT peaks as shown in the Figure 3(C). The peaks are close to those in linear electronic second harmonic generation spectrum as shown in Figure S3. This is likely due to the fact that the interfacial molecules are well ordered or partially ordered at the interface so that contributions from orientational broadening are greatly suppressed in the interface-specific 2D-EVSFG. On the other hand, for the vibrational mode of 1403.2 cm⁻¹, two ESA peaks show up at 566.2 nm and 550.0 nm, which are blue shifted with respect to their GSB counterparts. This blue shift can be ascribed to the anharmonicity of the vibronic potential energy surfaces for different vibronic states as discussed in the Supporting Information. As detailed in a theoretical study, (82) a shift of two-dimensional electronic-vibrational signals between ESA and GSB is expected if quadratic vibronic coupling is considered for coherent mode mixing. Our estimated quadratic vibronic coupling coefficient of 0.043 is actually very close to 0.038 chosen in that theoretical study, (82) for typical dye molecules.

Interfacial electronic-vibrational couplings at the initial photoexcitation of AP3. For electronic transitions within the Franck-Condon approximation, electronic transitions are independent of nuclear coordinates but related to vibrational manifolds on ground and excited state potentials. As a result, the couplings between electronic and vibrational degrees of freedom determine the vertical Franck-Condon factors. The Huang–Rhys factor, S, directly related to the displacement of the equilibrium positions of the nuclei, is a measure for the strength of the electron–vibration couplings in the Condon region. On the other hand, for the non-Condon excitation such as the Herzberg-Teller vibronic couplings, electronic transitions are dependent upon nuclear coordinates. 2D-EVSFG peaks are characteristic of specific vibrational modes coupled with electronic transitions in interfacial molecules. As such, peak intensity in 2D-EVSFG is sensitive not only to the Franck-Condon factors, but also to the non-Condon effect through intensity contributions from the first order or even higher order derivative of transition dipole moment with respect to the nuclear coordinates in electronic transitions.(82)

To further reveal the nuclear dependence of electronic transitions upon photoexcitation, we compared GSB 2D-EVSFG peaks from the vibronic transitions g0-e0' to g0-e'0'', as shown in Figure 3. At initial photoexcitation, the 2D-EVSFG experiments exhibited two separate GSB VT peaks at 573.4 nm and 556.8 nm with of an energy gap of 520.0 cm⁻¹. It was found that the vibronic transitions exhibit an intensity ratio of 1.01:1 at 573.4 nm (g0-e0') and 556.8 nm (g0-e'0'') in the ground state. Since the GSB 2D-EVSFG signal is proportional to $\mu^2_{gv,eu}\mu_{gv,gv'}\alpha_{gv',gv}$, the intensity

ratio for the two VT peaks is equal to $\mu^2_{g0,e0}$: $\mu^2_{g0,e0}$. Here, the VT at 573.4 nm is assumed to be the lowest transition (g0-e0') at the interface. This is a good approximation with the Franck-Condon transition. If the VT at 556.8 nm (g0-e'0'') is also the Franck-Condon excitation, this intensity ratio of the vibronic transitions would be 1:*S*. The Huang-Rhys factor *S* for the mode of 520.0 cm⁻¹ would be on the order of 1.01. However, our computations show that no significant Franck-Condon transition was found for the VT at 556.8 nm (g,0-e'0'') as displayed in Tables S1 & S2. Such a large value of *S* value is unlikely to originates from the Franck-Condon excitation. It was suggested that the Herzberg-Teller vibronic coupling might play an important role in the photoexcitation.

On the other hand, the ESA 2D-EVSFG intensity is proportional to $\mu^2_{gv,eu}\mu_{eu,eu'}\alpha_{eu',eu}$. The intensity ratio of the two VT transitions at 565.7 nm and 550.0 nm, is equal to $\mu^2_{g0,e0}\mu_{e0',e1'}:\mu^2_{g0,e0'}\mu_{e'0'',e'1''}$ in the excited state for the vibrational mode of 1402.4 cm⁻¹. Thus, we are able to extract $\mu_{e0',e1}:\mu_{e'0'',e'1''}$ for the vibronic transitions at 565.7 nm and 550.0 nm in the excited state since $\mu^2_{g0,e0}:\mu^2_{g0,e0'}$ was known from the GSB 2D-EVSFG peaks described above. With an intensity ratio of 2:1 at the two peaks from Figure 3, the $\mu_{e0',e1'}:\mu_{e'0'',e'1''}$ was found to be 1.41:1 for the vibrational mode of 1402.4 cm⁻¹. Therefore, the 2D-EVSFG spectra enable us to quantitatively compare vibrational transition strengths in the excited states of interfacial molecules.

Time-dependent 2D-EVSFG spectra. To reveal time evolution of the LE state of interfacial molecules of AP3, 2D-EVSFG spectra were taken for different waiting times T_w . Figure 4 shows 2D-EVSFG spectra of 20 μM AP3 at the air/water interface for four waiting times of 0 fs (A), 200 fs (B), 600 fs (C), and 1000 fs (D). At T_w =0 fs, only one positive peak initially occurs at 1403.2 cm⁻¹ along the vibrational axis. As the time goes on, additional two peaks start to appear at 1521.7 cm⁻¹ and 1585.5 cm⁻¹ for a waiting time of 200 fs. As the T_w increases, the 2D-EVSFG signals for the two peaks get stronger. These suggest that the LE state of the AP3 experiences change in nuclear geometry with time.

To further quantify time evolution of electronic-vibrational couplings, we chose to track time-dependent changes in the three positive regions of the time-dependent 2D-ESFG spectra for AP3. We integrated the areas for three vibrational peaks, including $1403.2 \pm 5.0 \text{ cm}^{-1}$, $1521.7 \pm 5.0 \text{ cm}^{-1}$, and $1585.5 \pm 5.0 \text{ cm}^{-1}$ from 540 nm to 575 nm. Figure 5 (A) shows kinetic behaviors of the three excited peaks. The lifetime for the vibrational mode of $1403.2 \pm 5.0 \text{ cm}^{-1}$ was found to be as short as 80 ± 5 fs. On the other hand, the time constants for the generation of the two vibrational modes at 1521.7 cm^{-1} and 1585.5 cm^{-1} in Figure 5 (B) are on the order of $406 \pm 21 \text{ fs}$ and $261 \pm 13 \text{ fs}$, respectively. The initial negative backgrounds for both the 1521.7 cm^{-1} and 1585.5 cm^{-1} peaks originate from the GSB contributions from their adjacent modes. These kinetic results suggest that

these high-frequency vibrations are strongly coupled with the fast relaxation of the excited state in AP3 at the interface.

Discussion

Interfacial electronic-vibrational couplings during the relaxation of excite states. Our timedependent 2D-EVSFG experiments demonstrated that the time evolution of the vibrational coordinates at 1530 cm⁻¹ and 1580 cm⁻¹ are accompanied with the relaxation process of the AP3 excited state. To understand how the two vibrational modes of 1530.0 cm⁻¹ and 1580.0 cm⁻¹ are coupled with the excited states of AP3, we carried out quantum chemistry calculations. As shown in Fig. 5 (C), an incident photon of ~2.2 eV (560 nm) pumps the molecule from its S₀ state to LE S₂ state directly, before the thermal relaxation narrows the vertical gap to 0.12 eV that facilitates the non-adiabatic $S_2 \rightarrow S_1$ transition. Subsequently, the S_1 state undergoes a pronounced thermal relaxation with a notable energy loss of 0.88 eV to reach the optimized S_1 structure, whose $S_1 \rightarrow S_0$ transition energy is as small as 0.19 eV. Finally, another non-adiabatic transition recovers the S₀ state albeit with an excited vibrational energy of 0.75 eV. The most striking feature observed on AP3's electronic structure change in the stepwise $S_2 \rightarrow S_1 \rightarrow S_0$ transition is the hole collapse with characteristic intramolecular charge transfer as illustrated in Fig. 5(D). Specifically, the wellextended hole across the aromatic backbone of AP3 in S_2 drastically shrinks to a dumbbell that is centered on the -N=N double bond in S₁. By contrast, the shape of the spatially delocalized electron remains nearly unchanged upon the $S_2 \rightarrow S_1$ transition. The hole collapse not only justifies the optically dark S₁ state due to its diminished transition dipole moment, but also suggests a distinct vibronic coupling at S_1 potential energy surface when compared to that at S_2 if one considers the sensitivity of electronic wavefunction with respect to molecular vibration. As listed in Table S1, our calculated oscillator strength for the $S_0 \rightarrow S_2$ transition at the optimized S_0 structure is close to unity, making S_2 the only optically bright state from the ground state. By contrast, the S_1 is only accessible through the thermal relaxation from S_2 . Interestingly, the oscillator strengths for both $S_2 \rightarrow S_0$ and $S_1 \rightarrow S_0$ transitions at the optimized excited-state structures are nearly zero, attesting AP3 as a fluorescence-free dye.

To understand the electronic-vibrational couplings of the intramolecular change transfer from S_2 to S_1 , we calculated the Huang-Rhys factors for all the normal modes with $S_k > 0.3$ in the $S_2 \rightarrow S_1$ transition as listed in Table S3. It was found that all the normal modes strongly coupled to the two electronic transitions are smaller than 1200 cm⁻¹, except for $v_{147}=1529.1$ cm⁻¹ and $v_{150}=1568.1$ cm⁻¹ during the $S_2 \rightarrow S_1$ transition. Both the vibrational modes are predominantly contributed by the two nitrogen atoms of the azo group demonstrated in Figure 5 (E). As listed in Table S3, the Huang-Rhys factors of the 1529.1 cm⁻¹ and 1568.1 cm⁻¹ modes for the $S_2 \rightarrow S_1$ transition are as large as

0.39 and 0.42, respectively. On the other hand, the couplings of the two modes for the $S_0 \rightarrow S_2$ transition did not occur in Table S2. In other words, the two strong vibrations around ~1550 cm⁻¹ are expected to appear in the time evolution of the 2D-EVSFG as confirmed by our experimental results. As a result, the strong electronic-vibrational couplings invalidate the Born-Oppenheimer approximation and thus promote the relaxation of AP3's S_2 to S_1 through a non-adiabatic manner. Our approach paves the way for the real-time monitoring of excited-state evolution at interfaces particularly for dye molecules with non-fluorescent charge-separated states as the intermediates upon thermal relaxation. For example, a dark charge-separated state was found to facilitate singlet fission and thus electron injection from a thin film of triisopropyl silylethynyl (TIPS)-pentacene to nanostructured TiO₂.(100) Therefore, a better understanding of the critical balance between singlet fission and charge separation both driven by vibronic coupling could be achieved at this molecule/semiconductor interface using our 2D-EVSFG.

Concluding Remarks

We have developed interface-specific two-dimensional electronic-vibrational SFG spectroscopy (2D-EVSFG) and demonstrated its applications to the excited-state dynamics of AP3 molecules at the air/water interface. The 2D-EVSFG experiments showed strong electronicvibrational couplings of interfacial AP3 molecules upon photoexcitation. Quantitative analyses of 2D-EVSFG peak intensity enabled us to reveal that the non-Condon effect accounts for the initial vibronic states at 573.4 nm and 556.8 nm of AP3 at the air/water interface. It was further found that the two vibronic states show different vibrational transition strengths. The 2D-EVSFG experiments also showed strong electronic-vibrational couplings of interfacial AP3 molecules in the relaxation of the excited states. Time-dependent 2D-EVSFG displayed that the relaxation of the LE state, S2, evolves with the changes in nuclear motions to a lower S₁ excited state. The time evolution of the excited state is strongly coupled with two high-frequency modes of 1529.1 cm⁻¹ and 1568.1 cm⁻¹. Quantum chemistry calculations further evidenced that both vibrational modes are predominantly contributed by the two nitrogen atoms of the azo group, and thus possess large Huang-Rhys factors for the $S_2 \rightarrow S_1$ transition. The strong electronic-vibrational couplings break the Born-Oppenheimer approximation and promote the relaxation of the S2 state of photoexcited AP3 to S1. The 2D-EVSFG experiments demonstrated the ability to correlate the initial excitation of the electronic-vibrational manifolds with the subsequent evolution of high-frequency vibrational modes at the interface.

The 2D-EVSFG spectroscopy combines the advantages of 2D-VSFG and 2D-ESFG, enabling us to couple the initial electronic absorption of vibronic transitions and subsequent time evolution of nuclear motions at interfaces and surfaces. The 2D-EVSFG technique provides a new approach to understand electronic-vibrational couplings of excited states at interfaces and surfaces. We

believe that this tool opens a new window for both chemists and physicists in the fields of interfacial and surface science as well as non-adiabatic dynamics theory.

Materials and Methods

2D-EVSFG Setup. A Ti: sapphire regenerative amplifier (800 nm, 100 fs, ~4 W, 1 kHz, Uptek Solution) was used for the generation of a visible pump, an IR beam, and an 800 nm picosecond pulse. A portion of 0.8 mJ from the fundamental light was used to pump a home-built noncollinear optical parametric amplifier (NOPA) for the visible pump. The output of the NOPA (centered at 560 nm, FWHM of 25 nm, 6.0 μJ) was compressed with a pair of prisms (LaK21, Newport) to 25-30 fs and characterized by a home-built frequency-resolved optical gating. A translating wedge-based identical pulses encoding system (TWINs) was introduced to generate a pair of phase-locked pump pulses with precise control over a relative time delay, following the literature reported from Cerullo and co-workers.(79, 101, 102) A detailed description of the TWINS is found in the Supporting Information. The rest of the fundamental light was directed to pump a TOPAS (Light conversion) to generate a mid-IR of 3 μJ. The narrowband and picosecond 800 nm light of 10 μJ was produced by a narrow-band filter with the residual of the 800 nm from the TOPAS. The time delay between the picosecond 800 nm and the mid-IR was set to be zero. A programable motorized translational stage (Klinger) was used to control the time delay, T_w , between the pump and the 800 nm/IR pulses.

A reflection geometry was used for 2D-EVSFG and VSFG experiments. The picosecond 800 nm and IR beams were combined with a dichroic mirror (ISP optics) for a collinear propagation. A one-inch CaF_2 lens with a focal length of 75 mm was applied to focus the two beams onto interfaces at an angle of 60° with respect to the surface normal. Both VSFG and 2D-EVSFG signals were collected in a reflection direction with energy and momentum conservations. The incident angle of the pump pulses was set at 50° with respect to the surface normal. The polarization of the two pump beams, 2D-EVSFG/SFG, 800 nm, and IR beams were set to be p-, p-, s-, s- and p- polarized, respectively. The IR beam path was protected with a sealed box and purged with dry air so that relative humidity was kept below 1%.

2D-EVSFG signals are generally weak, similar to those of 2D-ESFG.(79, 91) An optical chopper in the pump beam path was placed to synchronize pump-on and pump-off signals. The chopper ran at a working frequency of 500 Hz in an effort to synchronize with the laser system. A single-axis scanning Galvo mirror (Thorlabs) was also synchronized with the chopper to image the pump-on and pump-off on the CCD detector. It was found that the signals fall into two spectral strips onto the CCD detector, which was assembled by consolidating a vertically focused cylindrical lens of 25 cm with a horizontally focused cylindrical lens of 10 cm. The 2D-EVSFG signals were

detected by a spectrometer (Andor-2300i, Princeton Instrument) with a liquid nitrogen-cooled CCD (Princeton Instrument, back-illuminated 1300×400). A self-edited Labview program was compiled to control signal collection and data processing. The coherent time delay, τ_1 , was incremented in 0.32 fs time steps between 0 and 80 fs. Each data point was acquired for 10 seconds. Transient visible pump-VSFG probe were also acquired with the same setup except the two coherent pump lasers were set to be zero. A calibration of the pump wavelength and phases as well as determination of absolute time delay have been made as described in our early work in two-dimensional ESFG. (79, 91)

Simulation Details. The AP3 molecule was first optimized at its ground state, S_0 , by the density functional theory (DFT)(103) with B3LYP exchange-correlation functional(104, 105) and cc-PVTZ basis set.(106) Unless otherwise specified, all calculations were performed using NWCHEM,(107) an open-source simulation package. Subsequently, its excited-state optimized geometries at S_1 and S_2 were ascertained by the time-dependent density functional theory (TDDFT).(108) Then, for each of these three optimized structures, its vertical excitation energies of $\Delta E_{S_0 \to S_1}$ and $\Delta E_{S_0 \to S_2}$ were calculated by the quasiparticle self-consistent GW (QPSCGW) method(109) in conjunction with Bethe-Salpeter Equation (BSE) (110) using MOLGW software.(111) Finally, all normal modes at S_0 , S_1 , and S_2 were determined by diagonalizing the molecule's mass-weighted Hessian matrix before its Infrared and Raman spectra were resolved by a perturbation approach.(112)

Chemicals. The synthesis of AP3 was made in Figure S4 and modified by following the report in the literature.(113) A detailed description is found in the Supporting Information. The NMR spectrum of the AP3 compound is shown in Figure S5.

Data Availability. All relevant data, materials, protocols, computational details, and theoretical analysis are included in the manuscript and SI Appendix.

Acknowledgments

This material is based upon work supported by the National Science Foundation under Grant No. [2045084]. Y.R. is also grateful for Utah State University for the generous start-up fund. Computational resources were provided by the Argonne Leadership Computing Facilities at Argonne National Laboratory under Department of Energy contract DE-AC-06CH11357 and by the Extreme Science and Engineering Discovery Environment at Texas Advanced Computing Center under National Science Foundation contract TG-CHE130008.

References

- 1. F. Liu, G. J. Meyer, A Nuclear Isotope Effect for Interfacial Electron Transfer: Excited-State Electron Injection from Ru Ammine Compounds to Nanocrystalline TiO₂. *J Am Chem Soc* **127**, 824-825 (2005).
- 2. N. A. Anderson, T. Lian, Ultrafast electron transfer at the molecule-semiconductor nanoparticle interface. *Annu Rev Phys Chem* **56**, 491-519 (2005).
- 3. K. B. Eisenthal, Photochemistry and Photophysics of Liquid Interfaces by Second Harmonic Spectroscopy. *The Journal of Physical Chemistry* **100**, 12997-13006 (1996).
- 4. J. P. Gauyacq, A. G. Borisov, M. Bauer, Excited states in the alkali/noble metal surface systems: A model system for the study of charge transfer dynamics at surfaces. *Progress in Surface Science* **82**, 244-292 (2007).
- 5. Z. Gengeliczki, D. E. Rosenfeld, M. D. Fayer, Theory of interfacial orientational relaxation spectroscopic observables. *J Chem Phys* **132**, 244703 (2010).
- 6. Y. Rao, M. Xu, S. Jockusch, N. J. Turro, K. B. Eisenthal, Dynamics of Excited State Electron Transfer at a Liquid Interface Using Time-Resolved Sum Frequency Generation. *Chemical Physics Letters* **544**, 1-6 (2012).
- 7. E. A. McArthur, K. B. Eisenthal, Ultrafast excited-state electron transfer at an organic liquid/aqueous interface. *J Am Chem Soc* **128**, 1068-1069 (2006).
- 8. Y. Rao, D. Song, N. J. Turro, K. B. Eisenthal, Orientational motions of vibrational chromophores in molecules at the air/water interface with time-resolved sum frequency generation. *The Journal of Physical Chemistry B* **112**, 13572-13576 (2008).
- 9. D. Zimdars, J. I. Dadap, K. B. Eisenthal, T. F. Heinz, Femtosecond Dynamics of Solvation at the Air/Water Interface. *Chemical Physics Letters* **301**, 112-120 (1999).
- 10. R. S. Oliboni *et al.*, Vibronic Effects in the Ultrafast Interfacial Electron Transfer of Perylene-Sensitized TiO₂ Surfaces. *The Journal of Physical Chemistry C* **123**, 12599-12607 (2019).
- 11. D. E. Rosenfeld, Z. Gengeliczki, B. J. Smith, T. D. P. Stack, M. D. Fayer, Structural Dynamics of a Catalytic Monolayer Probed by Ultrafast 2D IR Vibrational Echoes. *Science* **334**, 634 (2011).
- 12. M. Jacobs *et al.*, Ultrafast charge transfer and vibronic coupling in a laser-excited hybrid inorganic/organic interface. *Advances in Physics: X* **5**, 1749883 (2020).
- 13. B. Xiang, Y. Li, C. H. Pham, F. Paesani, W. Xiong, Ultrafast Direct Electron Transfer at Organic Semiconductor and Metal Interfaces. *Sci Adv* **3**, e1701508 (2017).
- 14. A. V. Benderskii, J. Henzie, S. Basu, X. Shang, K. B. Eisenthal, Femtosecond Aqueous Solvation at a Positively Charged Surfactant/Water Interface. *The Journal of Physical Chemistry B* **108**, 14017-14024 (2004).
- 15. Y. Rao, N. J. Turro, K. B. Eisenthal, Solvation dynamics at the air/water interface with time-resolved sum-frequency generation. *The Journal of Physical Chemistry C* **114**, 17703-17708 (2010).

- 16. Y. R. Shen, Surface Properties Probed by Second Harmonic and Sum Frequency Generation. *Nature* **337**, 519-525 (1989).
- 17. P. B. Miranda, Y. R. Shen, Liquid interfaces: A Study by Sum-frequency Vibrational Spectroscopy. *Journal of Physical Chemistry B* **103**, 3292-3307 (1999).
- 18. K. B. Eisenthal, EQUILIBRIUM AND DYNAMIC PROCESSES AT INTERFACES BY 2ND HARMONIC AND SUM FREQUENCY GENERATION. *Annual Review of Physical Chemistry* **43**, 627-661 (1992).
- 19. K. B. Eisenthal, Liquid Interfaces Probed by Second-Harmonic and Sum-Frequency Spectroscopy. *Chem Rev* **96**, 1343-1360 (1996).
- G. L. Richmond, Molecular Bonding and Interactions at Aqueous Surfaces as Probed by Vibrational Sum Frequency Spectroscopy. *Chemical Reviews* 102, 2693-2724 (2002).
- 21. H.-F. Wang, W. Gan, R. Lu, Y. Rao, B.-H. Wu, Quantitative Spectral and Orientational Analysis in Surface Sum Frequency Generation Vibrational Spectroscopy (SFG-VS). *International Reviews in Physical Chemistry* **24**, 191-256 (2005).
- 22. F. M. Geiger, Second Harmonic Generation, Sum Frequency Generation, and X⁽³⁾: Dissecting Environmental Interfaces with a Nonlinear Optical Swiss Army Knife. *Annual Review of Physical Chemistry* **60**, 61-83 (2009).
- Z. Chen, Y. R. Shen, G. A. Somorjai, Studies of Polymer Surfaces by Sum Frequency Generation Vibrational Spectroscopy. *Annual Review of Physical Chemistry* 53, 437-465 (2002).
- 24. A. M. Jubb, W. Hua, H. C. Allen, Environmental chemistry at vapor/water interfaces: insights from vibrational sum frequency generation spectroscopy. *Annual review of physical chemistry* **63**, 107-130 (2012).
- 25. H. Arnolds, M. Bonn, Ultrafast Surface Vibrational Dynamics. *Surface Science Reports* **65**, 45-66 (2010).
- 26. C. Y. Wang, H. Groenzin, M. J. Shultz, Surface characterization of nanoscale TiO2 film by sum frequency generation using methanol as a molecular probe. *Journal of Physical Chemistry B* **108**, 265-272 (2004).
- 27. C. M. Johnson, S. Baldelli, Vibrational Sum Frequency Spectroscopy Studies of the Influence of Solutes and Phospholipids at Vapor/Water Interfaces Relevant to Biological and Environmental Systems. *Chem Rev* **114**, 8416-8446 (2014).
- 28. B. J. Berne, J. T. Fourkas, R. A. Walker, J. D. Weeks, Nitriles at Silica Interfaces Resemble Supported Lipid Bilayers. *Acc Chem Res* **49**, 1605-1613 (2016).
- 29. K. Y. Kung, P. Chen, F. Wei, Y. R. Shen, G. A. Somorjai, Sum-frequency generation spectroscopic study of CO adsorption and dissociation on Pt(111) at high pressure and temperature. *Surface Science* **463**, L627-L633 (2000).
- 30. M. Makarem, C. M. Lee, D. Sawada, H. M. O'Neill, S. H. Kim, Distinguishing Surface versus Bulk Hydroxyl Groups of Cellulose Nanocrystals Using Vibrational Sum Frequency Generation Spectroscopy. *The journal of physical chemistry letters* **9**, 70-75 (2017).

- 31. H. Vanselous, A. M. Stingel, P. B. Petersen, Interferometric 2D Sum Frequency Generation Spectroscopy Reveals Structural Heterogeneity of Catalytic Monolayers on Transparent Materials. *Journal of Physical Chemistry Letters* **8**, 825-830 (2017).
- 32. H. Y. Wang, T. Gao, W. Xiong, Self-Phase-Stabilized Heterodyne Vibrational Sum Frequency Generation Microscopy. *ACS Photonics* **4**, 1839-1845 (2017).
- 33. A. P. Moon *et al.*, Using Heterodyne-Detected Electronic Sum Frequency Generation To Probe the Electronic Structure of Buried Interfaces. *The Journal of Physical Chemistry C* **121**, 18653-18664 (2017).
- 34. J. E. Laaser, M. T. Zanni, Extracting Structural Information from the Polarization Dependence of One- and Two-Dimensional Sum Frequency Generation Spectra. *Journal of Physical Chemistry A* **117**, 5875-5890 (2013).
- 35. E. C. Yan, L. Fu, Z. Wang, W. Liu, Biological Macromolecules at Interfaces Probed by Chiral Vibrational Sum Frequency Generation Spectroscopy. *Chem Rev* **114**, 8471-8498 (2014).
- 36. J. F. Liljeblad, E. Tyrode, Vibrational sum frequency spectroscopy studies at solid/liquid interfaces: Influence of the experimental geometry in the spectral shape and enhancement. *The Journal of Physical Chemistry C* **116**, 22893-22903 (2012).
- 37. I. V. Stiopkin *et al.*, Hydrogen Bonding at the Water Surface Revealed by Isotopic Dilution Spectroscopy. *Nature* **474**, 192-195 (2011).
- 38. A. U. Chowdhury *et al.*, Flexible approach to vibrational sum-frequency generation using shaped near-infrared light. *Opt. Lett.* **43**, 2038-2041 (2018).
- 39. R. R. Kumal, H. Nguyenhuu, J. E. Winter, R. L. McCarley, L. H. Haber, Impacts of Salt, Buffer, and Lipid Nature on Molecular Adsorption and Transport in Liposomes As Observed by Second Harmonic Generation. *The Journal of Physical Chemistry C* **121**, 15851-15860 (2017).
- 40. D. Elsenbeck, S. K. Das, L. Velarde, Substrate influence on the interlayer electron—phonon couplings in fullerene films probed with doubly-resonant SFG spectroscopy. *Physical Chemistry Chemical Physics* **19**, 18519-18528 (2017).
- 41. N. G. Rey, D. D. Dlott, Studies of Electrochemical Interfaces by Broadband Sum Frequency Generation. *Journal of Electroanalytical Chemistry* **800**, 114-125 (2017).
- 42. T. C. Anglin, J. C. Conboy, Kinetics and thermodynamics of flip-flop in binary phospholipid membranes measured by sum-frequency vibrational spectroscopy. *Biochemistry* **48**, 10220-10234 (2009).
- 43. Y.-C. Wen *et al.*, Unveiling microscopic structures of charged water interfaces by surface-specific vibrational spectroscopy. *Physical review letters* **116**, 016101 (2016).
- 44. G. H. Deng *et al.*, Successive Adsorption of Cations and Anions of Water-1-Butyl-3-methylimidazolium Methylsulfate Binary Mixtures at the Air-Liquid Interface Studied by Sum Frequency Generation Vibrational Spectroscopy and Surface Tension Measurements. *Journal of Physical Chemistry C* **120**, 12032-12041 (2016).

- 45. Y. Ma *et al.*, Photodimerization Kinetics of a Styrylquinoline Derivative in Langmuir–Blodgett Monolayers Monitored by Second Harmonic Generation. *The Journal of Physical Chemistry C* **121**, 23541-23550 (2017).
- 46. R.-J. Feng *et al.*, Effect of Ca2+ to Sphingomyelin Investigated by Sum Frequency Generation Vibrational Spectroscopy. *Biophysical journal* **112**, 2173-2183 (2017).
- 47. W. Wu *et al.*, Understanding the Different Steps of Surfactant Adsorption at the Oil–Water Interface with Second Harmonic Generation. *The Journal of Physical Chemistry C* **120**, 6515-6523 (2016).
- 48. S. Liu *et al.*, Coverage dependence of methanol dissociation on TiO2 (110). *The journal of physical chemistry letters* **6**, 3327-3334 (2015).
- 49. S. Nihonyanagi, S. Yamaguchi, T. Tahara, Ultrafast Dynamics at Water Interfaces Studied by Vibrational Sum Frequency Generation Spectroscopy. *Chemical Reviews* **117**, 10665-10693 (2017).
- 50. Z. Liu, Y. Li, Q. Xu, H. Wang, W.-T. Liu, Coherent Vibrational Spectroscopy of Electrochemical Interfaces with Plasmonic Nanogratings. *The Journal of Physical Chemistry Letters* **11**, 243-248 (2020).
- 51. B. R. Watson, B. Doughty, T. R. Calhoun, Energetics at the Surface: Direct Optical Mapping of Core and Surface Electronic Structure in CdSe Quantum Dots Using Broadband Electronic Sum Frequency Generation Microspectroscopy. *Nano Letters* **19**, 6157-6165 (2019).
- 52. Z. Zhang *et al.*, Surface sum frequency generation spectroscopy on non-centrosymmetric crystal GaAs (001). *Surface Science* **664**, 21-28 (2017).
- 53. J. A. Carter, Z. Wang, D. D. Dlott, Ultrafast nonlinear coherent vibrational sum-frequency spectroscopy methods to study thermal conductance of molecules at interfaces. *Accounts of chemical research* **42**, 1343-1351 (2009).
- 54. Z. Wang *et al.*, Ultrafast Flash Thermal Conductance of Molecular Chains. *Science* **317**, 787-790 (2007).
- 55. Y. Rao, S.-Y. Hong, N. J. Turro, K. B. Eisenthal, Molecular Orientational Distribution at Interfaces Using Second Harmonic Generation. *The Journal of Physical Chemistry C* **115**, 11678-11683 (2011).
- 56. Y. Rao *et al.*, Molecular Rotation in 3 Dimensions at an Air/Water Interface Using Femtosecond Time Resolved Sum Frequency Generation. *J Chem Phys* **150**, 094709 (2019).
- 57. S. Marc *et al.*, Ultrafast energy flow in model biological membranes. *New Journal of Physics* **9**, 390 (2007).
- 58. S. Yamamoto, A. Ghosh, H. K. Nienhuys, M. Bonn, Ultrafast Inter- and Intramolecular Vibrational Energy Transfer Between Molecules at Interfaces Studied by Time- and Polarization-Resolved SFG Spectroscopy. *Phys Chem Chem Phys* **12**, 12909-12918 (2010).
- 59. J. Tan, B. Zhang, Y. Luo, S. Ye, Ultrafast Vibrational Dynamics of Membrane-Bound Peptides at the Lipid Bilayer/Water Interface. *Angew Chem Int Ed Engl* **56**, 12977-12981 (2017).

- 60. K. Sekiguchi, S. Yamaguchi, T. Tahara, Femtosecond time-resolved electronic sumfrequency generation spectroscopy: A new method to investigate ultrafast dynamics at liquid interfaces. *The Journal of chemical physics* **128**, 114715 (2008).
- 61. M. DelloStritto, S. M. Piontek, M. L. Klein, E. Borguet, Relating Interfacial Order to Sum Frequency Generation with Ab Initio Simulations of the Aqueous Al₂O₃(0001) and (1120) Interfaces. *The Journal of Physical Chemistry C* **122**, 21284-21294 (2018).
- 62. M. B. Raschke, M. Hayashi, S. H. Lin, Y. R. Shen, Doubly-resonant sum-frequency generation spectroscopy for surface studies. *Chemical Physics Letters* **359**, 367-372 (2002).
- 63. M. Hayashi, S. H. Lin, M. B. Raschke, Y. R. Shen, A Molecular Theory for Doubly Resonant IR–UV-vis Sum-Frequency Generation†. *The Journal of Physical Chemistry A* **106**, 2271-2282 (2002).
- 64. S. H. Lin, A. A. Villaeys, Theoretical description of steady-state sum-frequency generation in molecular adsorbates. *Phys Rev A* **50**, 5134-5144 (1994).
- 65. R. Venkatramani, S. Mukamel, Dephasing-induced vibronic resonances in difference frequency generation spectroscopy. *J Phys Chem B* **109**, 8132-8143 (2005).
- 66. J. C. Vallet, A. J. Boeglin, J. P. Lavoine, A. A. Villaeys, Doubly resonant sumfrequency generation from molecules with general harmonic potential surfaces. *Chemical Physics Letters* **241**, 203-208 (1995).
- 67. J. C. Vallet, A. J. Boeglin, J. P. Lavoine, A. A. Villaeys, Vibronic mode couplings in adsorbed molecules analyzed by doubly resonant sum-frequency generation. *Phys Rev A* **53**, 4508-4518 (1996).
- 68. J. Y. Huang, Y. R. Shen, Theory of doubly resonant infrared-visible sum-frequency and difference-frequency generation from adsorbed molecules. *Phys Rev A* **49**, 3973-3981 (1994).
- 69. D. Wu, G. H. Deng, Y. Guo, H. F. Wang, Observation of the interference between the intramolecular IR-visible and visible-IR processes in the doubly resonant sum frequency generation vibrational spectroscopy of Rhodamine 6G adsorbed at the air/water interface. *J Phys Chem A* **113**, 6058-6063 (2009).
- 70. M. Raab *et al.*, Doubly resonant sum frequency spectroscopy of mixed photochromic isomers on surfaces reveals conformation-specific vibronic effects. *J Chem Phys* **150**, 114704 (2019).
- 71. B. Busson, Doubly resonant SFG and DFG spectroscopies: An analytic model for data analysis including distorted and rotated vibronic levels. I. Theory. *The Journal of Chemical Physics* **153**, 174701 (2020).
- 72. J. A. McGuire, Y. R. Shen, Ultrafast vibrational dynamics at water interfaces. *Science* **313**, 1945-1948 (2006).
- 73. J. Bredenbeck, A. Ghosh, M. Smits, M. Bonn, Ultrafast two dimensional-infrared spectroscopy of a molecular monolayer. *J Am Chem Soc* **130**, 2152-2153 (2008).

- 74. Z. Zhang, L. Piatkowski, H. J. Bakker, M. Bonn, Ultrafast vibrational energy transfer at the water/air interface revealed by two-dimensional surface vibrational spectroscopy. *Nat Chem* **3**, 888-893 (2011).
- 75. P. C. Singh, S. Nihonyanagi, S. Yamaguchi, T. Tahara, Ultrafast vibrational dynamics of water at a charged interface revealed by two-dimensional heterodyne-detected vibrational sum frequency generation. *J Chem Phys* **137**, 094706 (2012).
- 76. W. Xiong, J. E. Laaser, R. D. Mehlenbacher, M. T. Zanni, Adding a Dimension to the Infrared Spectra of Interfaces Using Heterodyne Detected 2D Sum-Frequency Generation (HD-2D-SFG) Spectroscopy. *Proceedings of the National Academy of Sciences* **108**, 20902-20907 (2011).
- 77. J. Wang *et al.*, Short-Range Catalyst–Surface Interactions Revealed by Heterodyne Two-Dimensional Sum Frequency Generation Spectroscopy. *The Journal of Physical Chemistry Letters* **6**, 4204-4209 (2015).
- 78. M. Schleeger, M. Grechko, M. Bonn, Background-Free Fourth-Order Sum Frequency Generation Spectroscopy. *The Journal of Physical Chemistry Letters* **6**, 2114-2120 (2015).
- 79. G.-H. Deng, Y. Qian, Q. Wei, T. Zhang, Y. Rao, Interface-Specific Two-Dimensional Electronic Sum Frequency Generation Spectroscopy. *The Journal of Physical Chemistry Letters* **11**, 1738-1745 (2020).
- 80. T. A. Oliver, N. H. Lewis, G. R. Fleming, Correlating the motion of electrons and nuclei with two-dimensional electronic-vibrational spectroscopy. *Proc Natl Acad Sci U S A* **111**, 10061-10066 (2014).
- 81. J. D. Gaynor, T. L. Courtney, M. Balasubramanian, M. Khalil, Fourier transform two-dimensional electronic-vibrational spectroscopy using an octave-spanning mid-IR probe. *Opt Lett* **41**, 2895-2898 (2016).
- 82. J. D. Gaynor, M. Khalil, Signatures of vibronic coupling in two-dimensional electronic-vibrational and vibrational-electronic spectroscopies. *J Chem Phys* **147**, 094202 (2017).
- 83. T. A. Oliver, G. R. Fleming, Following Coupled Electronic-Nuclear Motion through Conical Intersections in the Ultrafast Relaxation of beta-Apo-8'-carotenal. *J Phys Chem B* **119**, 11428-11441 (2015).
- 84. N. H. Lewis, H. Dong, T. A. Oliver, G. R. Fleming, Measuring correlated electronic and vibrational spectral dynamics using line shapes in two-dimensional electronic-vibrational spectroscopy. *J Chem Phys* **142**, 174202 (2015).
- 85. H. Dong, N. H. Lewis, T. A. Oliver, G. R. Fleming, Determining the static electronic and vibrational energy correlations via two-dimensional electronic-vibrational spectroscopy. *J Chem Phys* **142**, 174201 (2015).
- N. H. Lewis, H. Dong, T. A. Oliver, G. R. Fleming, A method for the direct measurement of electronic site populations in a molecular aggregate using twodimensional electronic-vibrational spectroscopy. *J Chem Phys* 143, 124203 (2015).

- 87. N. H. C. Lewis *et al.*, Observation of Electronic Excitation Transfer Through Light Harvesting Complex II Using Two-Dimensional Electronic-Vibrational Spectroscopy. *J Phys Chem Lett* **7**, 4197-4206 (2016).
- 88. N. H. Lewis, G. R. Fleming, Two-Dimensional Electronic-Vibrational Spectroscopy of Chlorophyll a and b. *J Phys Chem Lett* **7**, 831-837 (2016).
- 89. J. D. Gaynor, J. Sandwisch, M. Khalil, Vibronic coherence evolution in multidimensional ultrafast photochemical processes. *Nat Commun* **10**, 5621 (2019).
- 90. E. C. Wu *et al.*, Two-dimensional electronic-vibrational spectroscopic study of conical intersection dynamics: an experimental and electronic structure study. *Phys Chem Chem Phys* **21**, 14153-14163 (2019).
- 91. G.-H. Deng *et al.*, Development of interface-/surface-specific two-dimensional electronic spectroscopy. *Review of Scientific Instruments* **92**, 023104 (2021).
- 92. M. Cho, *Two-dimensional optical spectroscopy* (CRC press, 2009).
- 93. J. E. Laaser, W. Xiong, M. T. Zanni, Time-Domain SFG Spectroscopy Using Mid-IR Pulse Shaping: Practical and Intrinsic Advantages. *The Journal of Physical Chemistry B* **115**, 2536-2546 (2011).
- 94. M. Khalil, N. Demirdoven, A. Tokmakoff, Obtaining absorptive line shapes in two-dimensional infrared vibrational correlation spectra. *Phys Rev Lett* **90**, 047401 (2003).
- 95. S. Y. Lee, D. Zhang, D. W. McCamant, P. Kukura, R. A. Mathies, Theory of femtosecond stimulated Raman spectroscopy. *J Chem Phys* **121**, 3632-3642 (2004).
- 96. D. W. McCamant, P. Kukura, S. Yoon, R. A. Mathies, Femtosecond broadband stimulated Raman spectroscopy: Apparatus and methods. *Rev Sci Instrum* **75**, 4971-4980 (2004).
- 97. K. C. Wilson, B. Lyons, R. Mehlenbacher, R. Sabatini, D. W. McCamant, Two-dimensional femtosecond stimulated Raman spectroscopy: Observation of cascading Raman signals in acetonitrile. *J Chem Phys* **131**, 214502 (2009).
- 98. S. R. Ellis, D. P. Hoffman, M. Park, R. A. Mathies, Difference Bands in Time-Resolved Femtosecond Stimulated Raman Spectra of Photoexcited Intermolecular Electron Transfer from Chloronaphthalene to Tetracyanoethylene. *J Phys Chem A* **122**, 3594-3605 (2018).
- 99. Z. Zhang, A. Huerta-Viga, H. S. Tan, Two-dimensional electronic-Raman spectroscopy. *Opt Lett* **43**, 939-942 (2018).
- 100. N. A. Pace *et al.*, Dynamics of singlet fission and electron injection in self-assembled acene monolayers on titanium dioxide. *Chem Sci* **9**, 3004-3013 (2018).
- 101. D. Brida, C. Manzoni, G. Cerullo, Phase-Locked Pulses For Two-Dimensional Spectroscopy by a Birefringent Delay Line. *Opt. Lett.* **37**, 3027-3029 (2012).
- 102. J. Réhault, M. Maiuri, A. Oriana, G. Cerullo, Two-Dimensional Electronic Spectroscopy with Birefringent Wedges. *Review of Scientific Instruments* **85**, 123107 (2014).

- 103. P. Hohenberg, W. Kohn, Inhomogeneous Electron Gas. *Physical Review* **136**, B864-B871 (1964).
- 104. A. D. Becke, Density functional thermochemistry. III. The role of exact exchange. *The Journal of Chemical Physics* **98**, 5648-5652 (1993).
- 105. C. Lee, W. Yang, R. G. Parr, Development of the Colle-Salvetti correlation-energy formula into a functional of the electron density. *Physical Review B* **37**, 785-789 (1988).
- D. E. Woon, T. H. Dunning, Gaussian basis sets for use in correlated molecular calculations. IV. Calculation of static electrical response properties. *The Journal of Chemical Physics* 100, 2975-2988 (1994).
- 107. E. Aprà *et al.*, NWChem: Past, present, and future. *The Journal of Chemical Physics* **152**, 184102 (2020).
- 108. M. E. Casida, M. Huix-Rotllant, Progress in Time-Dependent Density-Functional Theory. *Annual Review of Physical Chemistry* **63**, 287-323 (2012).
- 109. M. van Schilfgaarde, T. Kotani, S. Faleev, Quasiparticle Self-Consistent \$GW\$ Theory. *Physical Review Letters* **96**, 226402 (2006).
- 110. E. E. Salpeter, H. A. Bethe, A Relativistic Equation for Bound-State Problems. *Physical Review* **84**, 1232-1242 (1951).
- 111. F. Bruneval *et al.*, molgw 1: Many-body perturbation theory software for atoms, molecules, and clusters. *Computer Physics Communications* **208**, 149-161 (2016).
- 112. F. W. Aquino, G. C. Schatz, Time-Dependent Density Functional Methods for Raman Spectra in Open-Shell Systems. *The Journal of Physical Chemistry A* **118**, 517-525 (2014).
- 113. M. Nuriya *et al.*, Multimodal two-photon imaging using a second harmonic generation-specific dye. *Nat Commun* **7**, 11557 (2016).

Figures

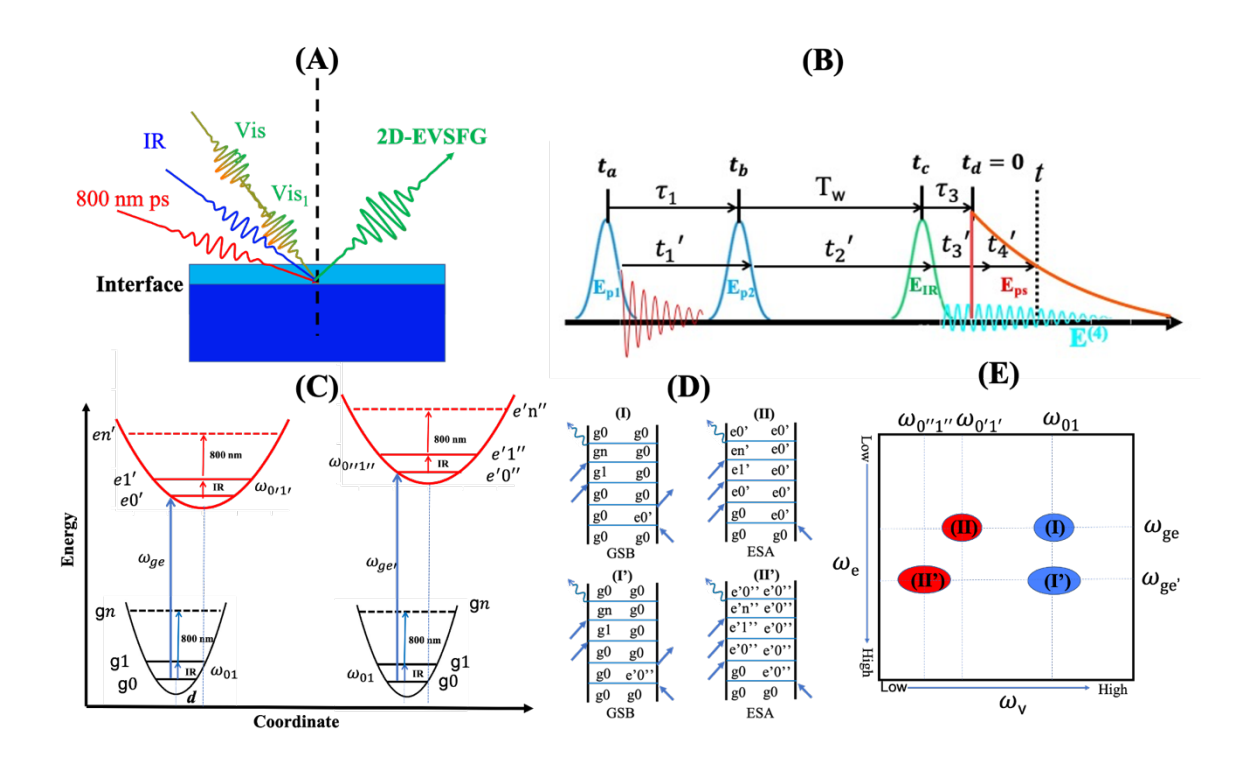


Figure 1. (A) An experimental configuration of the incident lasers and detection signal for interfaces in a reflection-geometry 2D-EVSFG. (B) A pulse sequence for 2D-EVSFG. (C) Potential energy surfaces for two vibronic transitions. gn, en, and e, and e, represent virtual states for S_0 and the two vibronic states, respectively. (D) Four rephasing Feynman pathways for 2D-EVSFG. (E) Schematic 2D-EVSFG peaks for the four pathways in (D). The blue and red colors represent negative GSB and positive ESA.

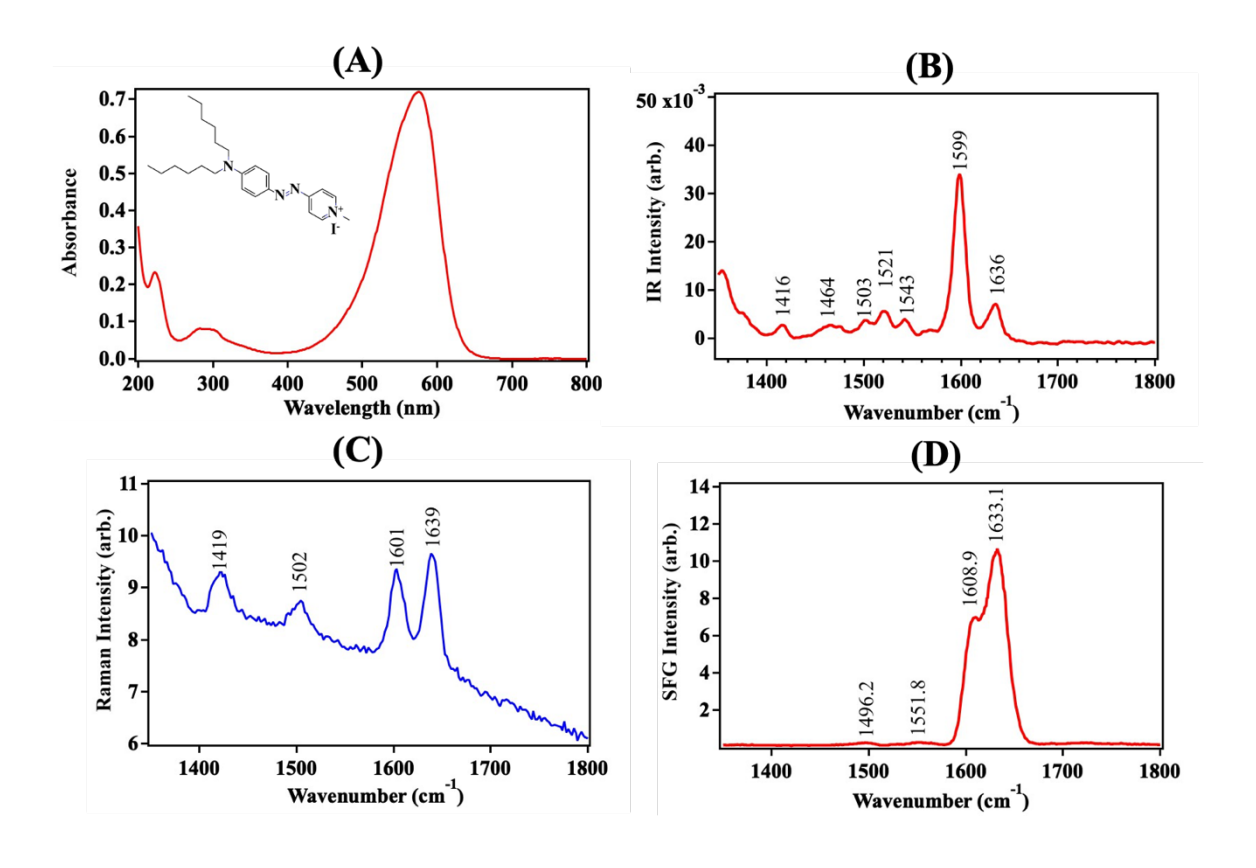


Figure 2. A) UV-vis spectrum of 100 μ M AP3 in water. The inset is the chemical structure of AP3. B) IR spectrum of AP3. C) Raman spectrum of 2 mM AP3 in D₂O. D) SFG spectra of 20 μ M AP3 at the air/water interface.

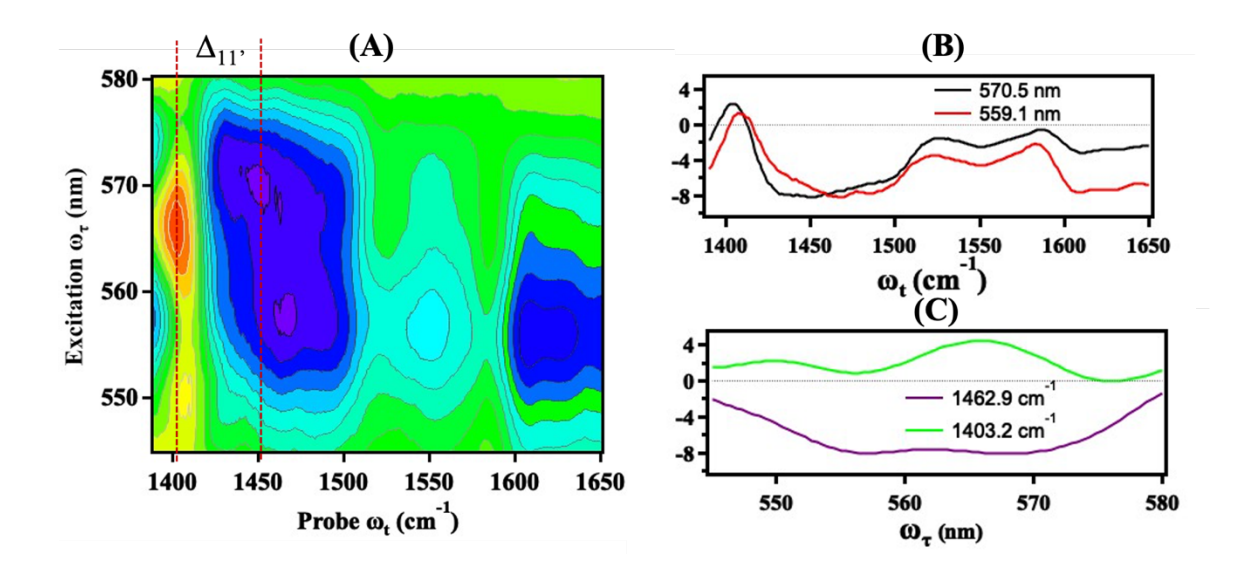


Figure 3. (A) 2D-EVSFG spectra of 20 μM AP3 at the air/water interface at a waiting time of T_w =20 fs. Δ_{11} is the spectral shift of vibrational transitions between the GSB and ESA. (B) Sliced spectra at 570.5 nm and 559.1 nm along the vibrational axis. (C) Sliced spectra at 1462.9 cm⁻¹ and 1403.2 cm⁻¹ along the electronic axis. At the GSB peak of 1462.9 cm⁻¹, two excitation wavelength peaks show up at 570.5 nm and 559.1 nm. On the other hand, at the ESA peak of 1403.2 cm⁻¹, two excitation wavelength peaks show up at 566.2 nm and 550.0 nm.

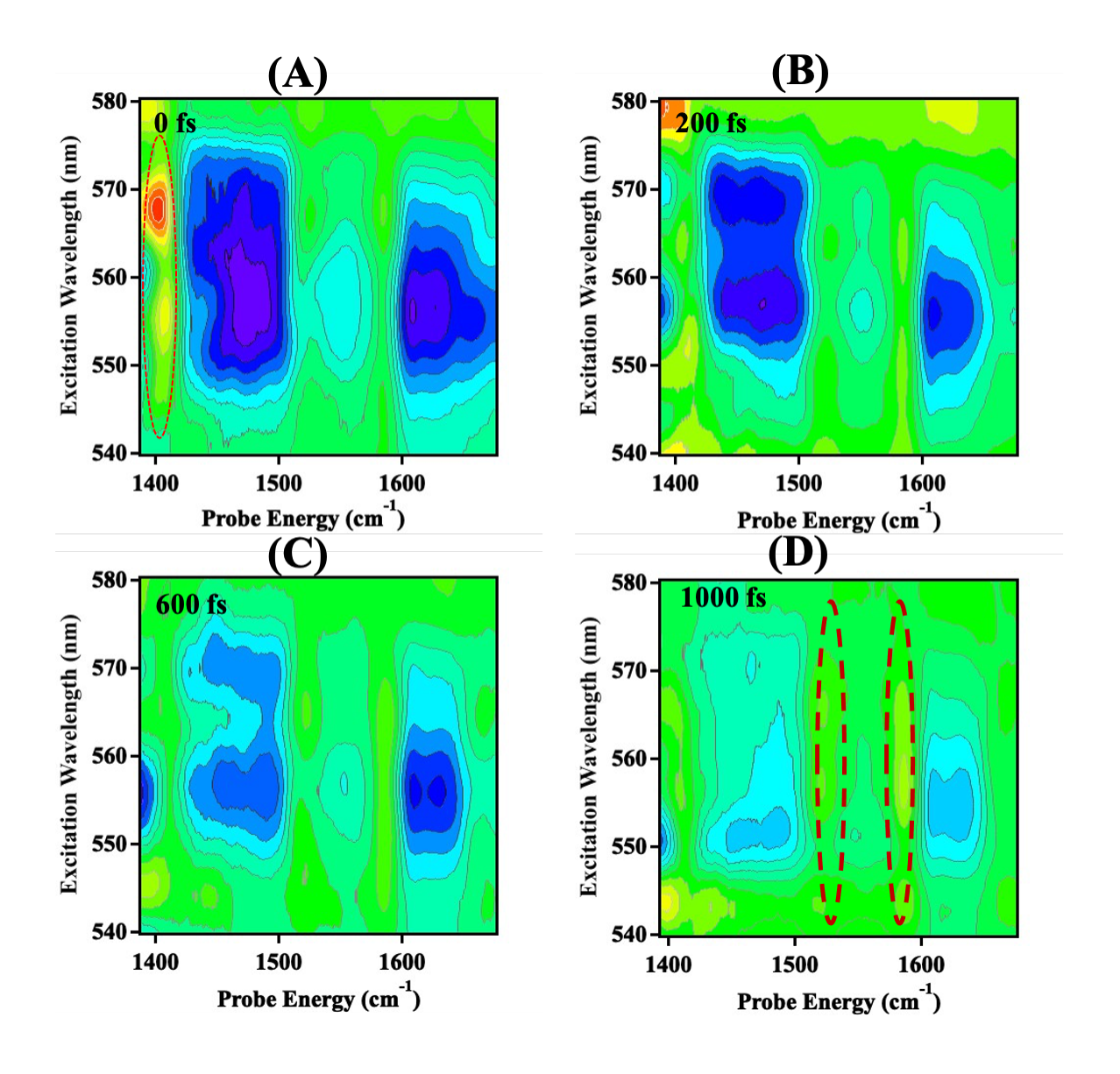


Figure 4. 2D-EVSFG spectra of 20 μ M AP3 at the air/water interface for four waiting times of 0 fs (A), 200 fs (B), 600 fs (C), and 1000 fs (D). The positive peak at 1403.2 cm⁻¹ diminishes with the waiting time, T_w , while the positive peaks at 1521.7 cm⁻¹ and 1585.5 cm⁻¹ start to show up with the waiting time, T_w . The color scale for the spectra is the same as that in Figure 3A.

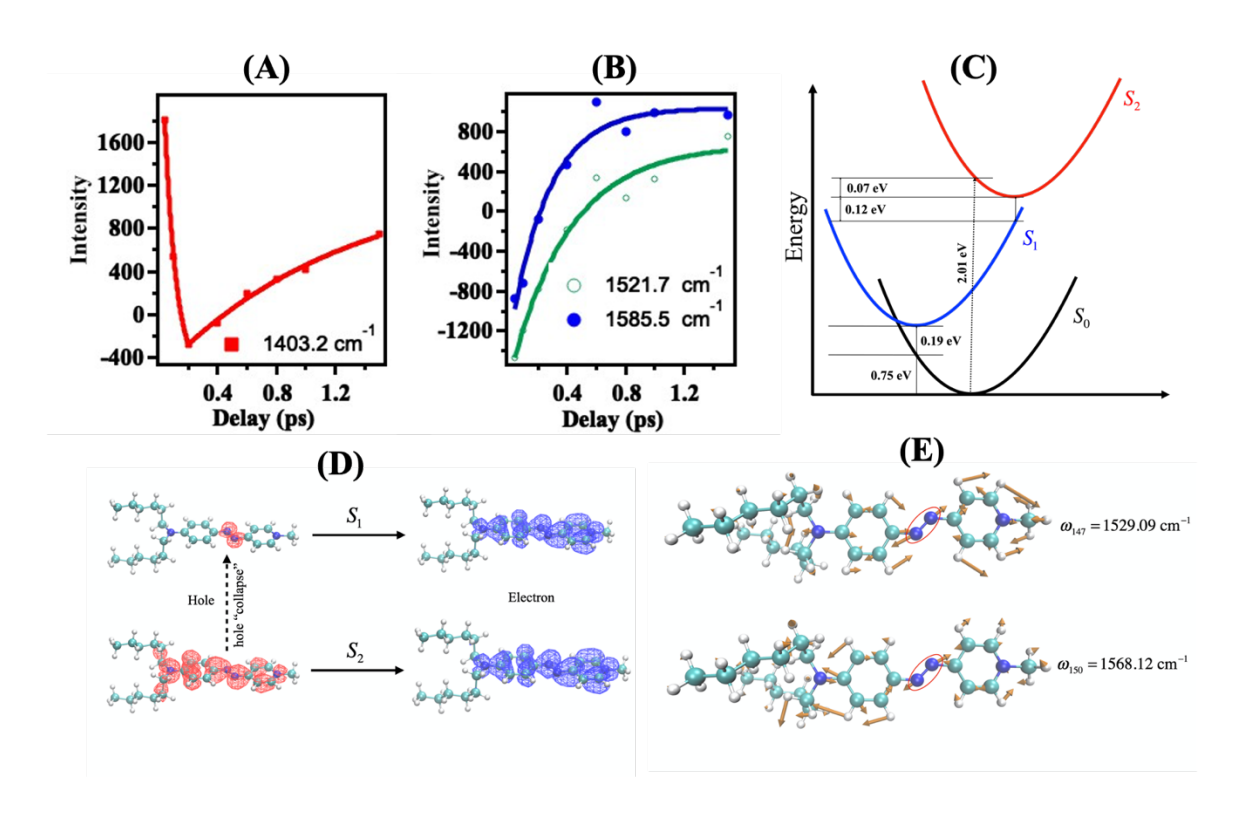


Figure 5. Evolution of integration areas for three vibrational peaks, including 1403.2 ± 5.0 cm⁻¹(A) ,1521.7 \pm 5.0 cm⁻¹, and 1585.5 ± 5.0 cm⁻¹ (B) from 540 nm to 575 nm, as a function of the waiting time, T_w . C) Energy diagram of electronic states for AP3. D) Simulated iso-surfaces of hole and electron for the S_1 and S_2 states of the AP3 molecule upon excitation from its ground state, S_0 . E) Visualization of two vibrational modes at 1529.09 and 1568.12 cm⁻¹ for the vibronic coupling between S_2 and S_1 .